OPEN

In-situ device integration of large-area patterned organic nanowire arrays for high-performance optical sensors

Yiming Wu[1], Xiujuan Zhang[1], Huanhuan Pan[1], Wei Deng[1], Xiaohong Zhang[2], Xiwei Zhang[1] & Jiansheng Jie[1]

[1]Institute of Functional Nano & Soft Materials (FUNSOM) and Jiangsu Key Laboratory for Carbon-Based Functional Materials & Devices, Soochow University, Suzhou Jiangsu, 215123, P. R. China, [2]Nano-organic Photoelectronic Laboratory and Key Laboratory of Photochemical Conversion and Optoelectronic Materials, Technical Institute of Physics and Chemistry, Chinese Academy of Sciences (CAS), Beijing, 100190, P. R. China.

Single-crystalline organic nanowires (NWs) are important building blocks for future low-cost and efficient nano-optoelectronic devices due to their extraordinary properties. However, it remains a critical challenge to achieve large-scale organic NW array assembly and device integration. Herein, we demonstrate a feasible one-step method for large-area patterned growth of cross-aligned single-crystalline organic NW arrays and their in-situ device integration for optical image sensors. The integrated image sensor circuitry contained a 10×10 pixel array in an area of 1.3×1.3 mm^2, showing high spatial resolution, excellent stability and reproducibility. More importantly, 100% of the pixels successfully operated at a high response speed and relatively small pixel-to-pixel variation. The high yield and high spatial resolution of the operational pixels, along with the high integration level of the device, clearly demonstrate the great potential of the one-step organic NW array growth and device construction approach for large-scale optoelectronic device integration.

S emiconductor nanowires (NWs) have gained considerable attention in the past years because of their extraordinary properties[1–3]. They are promising building blocks for future high-performance and high-integration nanodevices for electronics, optoelectronics, sensors, and energy science[4,5]. The capability of assembling NWs rationally in an orientation-, dimensionality-, and location-controlled manner is vital in tuning their properties toward high-integration nanodevices[6,7]. Aligned growth of inorganic NW arrays is usually achieved on lattice matched substrates *via* a vapor-liquid-solid (VLS) process with metallic catalysts involved[8,9]. Limited by the high growth temperature ($>400°$C) requirement, the patterned growth and device integration of inorganic NW arrays have to be separated into different stages, which inevitably increases the complexity of the device integration and degrades the reproducibility of the devices.

Single-crystalline small molecular organic semiconductor NWs have attracted much attention because of their strikingly different electronic and optical properties from their inorganic counterparts as well as much more flexibility and diversity in material design and property manipulation[10–12]. Some unique applications have been successfully achieved from organic semiconductor NWs, such as organic photovoltaics (OPVs)[13], optical wave-guides and lasers[14], and field-effect transistors[15,16], which demonstrate great potential as building blocks for the next generation of miniaturized electronic and optoelectronic devices. In particular, the low growth temperature ($<200°$C) of organic NWs also makes the aligned growth of NWs and in-situ device integration possible. Great efforts have been devoted to the large-scale growth of organic NW arrays with good alignment and high controllability to achieve expected performances. Anodic aluminum oxide (AAO) and grating templated methods have been demonstrated to be effective for the aligned growth of organic NW arrays[17,18]. In addition, geometrically or chemically modifying the substrates with high surface energy are utilized to induce patterned growth of organic NW arrays on selective areas[19,20]. Our group previously developed an evaporation-induced self-assembly method to facilitate the alignment and patterning of organic NWs[21–23]. However, few studies so far have been concerned about promoting the application of the assembled organic NW arrays for functional integrated devices, possibly due to the difficulties in achieving precise patterning on designated locations or the complicated post-processing of the NW manipulating/alignment for integration[24–26].

Herein, we demonstrated simultaneous patterned growth and device integration of cross-aligned single-crystalline organic NW arrays for optical image sensors in large-area. Cross-aligned NW arrays can selectively grow on gold (Au) film-coated areas induced by the high surface energy. By manipulating the Au electrode geometries on the substrate by photolithography, patterned growth of NW arrays and in-situ device integration were achieved. The circuitry can function as an image sensor with a high spatial resolution. Notably, the unique cross-aligned NW array structure offers integrated devices with a strong light-trapping effect and extended light absorption length, which makes high-performance optical sensors possible. As expected, 100% of the image pixels operated well, which surpassed the previous reports on image sensors fabricated from the parallel-aligned inorganic NW arrays whose yield usually lower than 80%[27,28]. The integrated devices also exhibited excellent stability and reproducibility with small pixel-to-pixel variation, which was attributed to the high uniformity and high contact quality of the crossed NW arrays with the Au electrodes. The high yield and high spatial resolution of the operational pixels, along with the high integration level of our device, demonstrate the great potential of organic NW arrays for use in the construction of large-scale high-performance functional integrated devices.

Results and discussion

Figure 1a shows the schematic illustration of the growth process of cross-aligned copper phthalocyanine (CuPc) NW arrays. Au-coated silicon (Si) substrates were placed at downstream positions with ~20 cm away from the source powder. Scanning electron microscope (SEM) images in Figure 1b and 1c demonstrated that NW arrays were formed on the substrates with high density, large-area uniformity, and perfect crossed alignment. All the NWs are straight and distinct from each other with an average alignment angle of ~70° (inset in Figure 1c) and they have a uniform diameter/length of about 100–300 nm/~4 μm, respectively. It should also be noted that all the NWs grow from the Au film surface and spread across a large area over the entire substrate (Figure 1d). Contact angle detection indicates that the CuPc NW arrays are hydrophobic with a contact angle of ~120° with water (inset in Figure 1d). For transmission electron microscope (TEM) observation, a thin Si_3N_4 membrane (thickness 50 nm)-coated Si substrate with an opening Si window of 500 μm × 500 μm was used to replace the conventional copper (Cu) grid. A 6 nm Au film was deposited on the substrate to facilitate the direct growth of NW arrays on the Si_3N_4 membrane. Figure 1e shows the typical TEM image, the NW has smooth surface with uniform diameter along the length, revealing the high quality of the CuPc NWs. Moreover, Au nanoparticle (NP) is visible at the starting point of the NW growth (Inset in Figure 1e), which is consistent with the SEM observations. High-resolution TEM (HRTEM) and selected-area electron diffraction (SAED) observations reveal that the CuPc NWs are α-phase single crystalline (Figure 1f and 1g). The interplanar spacing of 12.5 Å indicates that the NWs have (002) side surfaces, while the growth orientation is determined to be [010] along the b-axis. Interestingly, the analysis of the NWs grown on different Au NPs does not show any clear trend or correlation with the NP shape. The control experiments also demonstrate that if bare Si wafer with no Au film coating was used as the depositing substrate, the resulting NWs were not free standing but instead, lay flat on the substrate, as shown in Figure S1a and S1b. While, when the Au-coated Si wafer was replaced with an Au-coated SiO_2/Si wafer as the depositing substrate, cross-aligned NW arrays were still formed (Figure S2), indicating that aligned growth of NWs is not determined by the nature of the substrates. All these results suggest that Au film has a critical function in the cross-aligned growth of NWs, but may only serve as the active sites for NW nucleation due to the large surface energy, as well as direct the subsequent aligned growth. Besides Au film, Ag film is also observed to be capable of directing
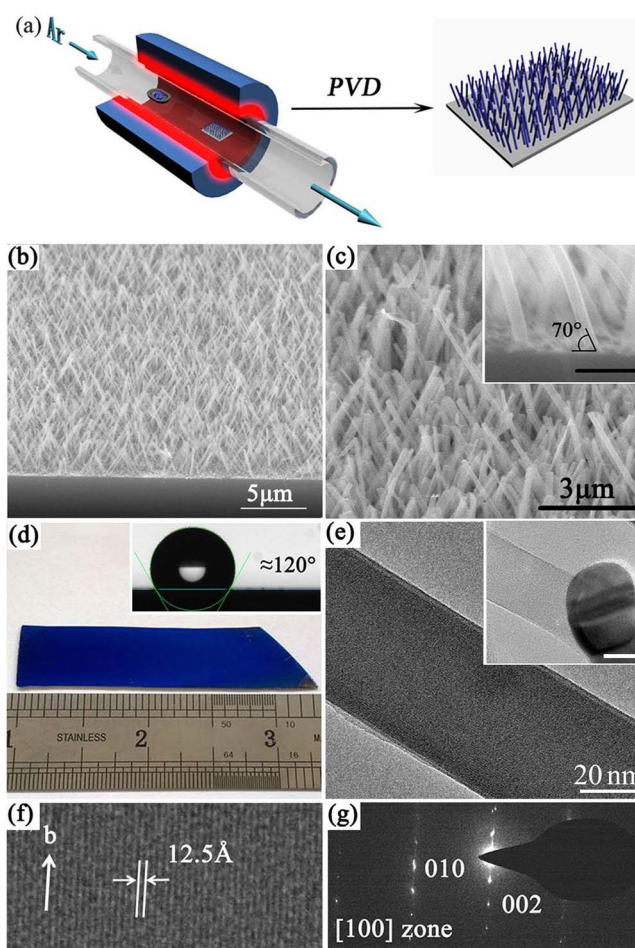
Figure 1 | (a) Schematic illustration of the setup for CuPc NW array growth. (b), (c) Tilted view SEM images of CuPc NW array grown on Au-coated Si substrate under different magnifications. The inset in (c) is an enlarged SEM image of the foot of the NW array, scale bar = 500 nm. (d) Photograph of a sample, revealing the large-area growth of the CuPc NW array over the entire substrate. The inset in (d) shows the contact angle measurement of a water drop with CuPc NW array. The contact angle was deduced to be ~120°. (e) Typical low-resolution TEM image of CuPc NWs grown on Si_3N_4 membrane. Inset shows the TEM image of a CuPc NW with an Au NP at the end, scale bar = 20 nm. (f) HRTEM image of a single α-CuPc NW. (g) SAED pattern of the α-CuPc NW. The SAED pattern is indexed for a monoclinic α-CuPc NW down the [100] zone axis.

the aligned growth of CuPc NW array (Figure S3). Moreover, this method exhibits large flexibility and can be extended to other organic molecules for their NW arrays growth. Figure S4a–S4c depict the SEM images of perylene-3, 4, 9, 10-tetracarboxylic acid dianhydride (PTCDA) and copper hexadecafluoro-phthalocyanine (F_{16}CuPc) NW arrays, respectively, prepared by using Au NPs as templates. The above results unambiguously demonstrate the excellent versatility of the metal NP-templated method for organic NW array growth.

We note that all the CuPc NWs have a tilted alignment on the substrate, which is much different with previous report on 1,5-diaminoanthraquinone (DAAQ) NWs[29], in which vertically aligned NWs were usually obtained on smooth substrates. To gain more insight into the growth mechanism of the cross-aligned CuPc NWs, morphology evolution at different growth stages was further investigated, as shown in Figure 2. It is seen that the Au NP was surrounded by an organic wetting layer at early growth stage (Figure 2a). However, the following NW nucleation tended to occur
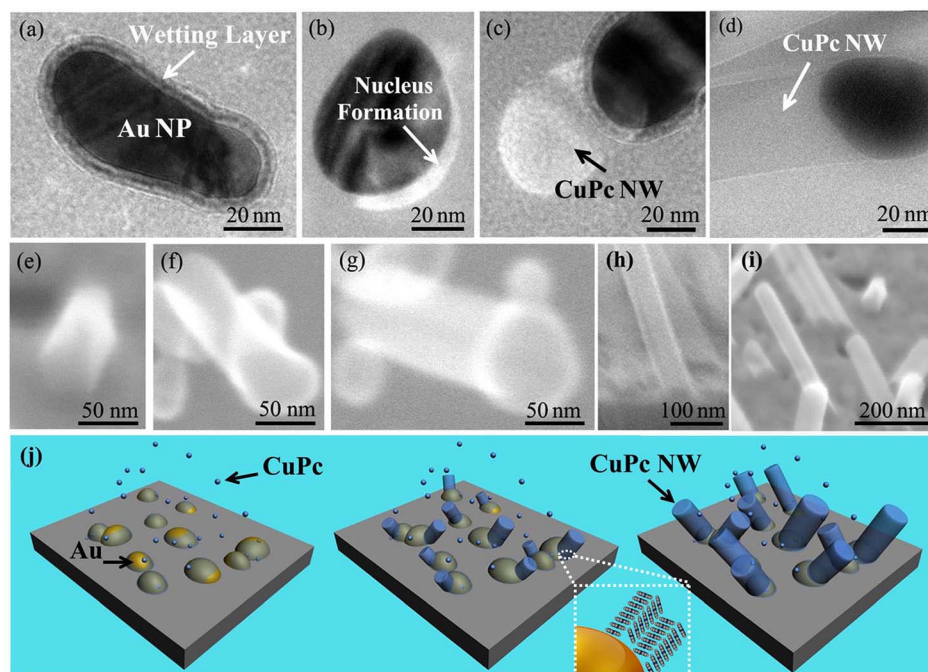
Figure 2 | (a) TEM image of an Au NP at early growth stage. CuPc wetting layer can be observed outside of the Au NP. (b) CuPc nucleation happens at the edge of Au NP. (c) Growth of CuPc NW at the side surface of Au NP. (d) CuPc NW after long time growth. (e)–(i) SEM images of the CuPc NWs at different growth stages. (j) Schematic illustration shows the growth process of the tilted CuPc NWs.

at the edge, rather than on the top of the Au NP, as shown in Figure 2b and Figure S5. This could be attributed to the higher surface energy at the corner position of Au NP with Si substrate. With the increase of growth time, Figure 2c, the NW nucleus would extend along the π-π stacking direction of CuPc, eventually forming the long organic NW (Figure 2d). SEM images in Figure 2e–2i also confirm the proposed growth mechanism. Since the NW always grow from the edges of Au NPs, tilted NWs should be obtained due to the curved surface of Au NPs, as illustrated in Figure 2j, giving rise to an approximated angle of $\sim 70^\circ$ for the NWs. By contrast, in previous work[29], smooth substrates were used as the growth substrates and a layer of vertically aligned, elongated DAAQ NPs were formed at the early state of the vapor transport, which then acted as the seeds for the epitaxial overgrowth of the NWs, leading to the vertical alignment of the NWs on smooth substrates.

Motivated by the above observations that Au film directed the aligned growth of NWs, we adopted photolithography patterning technique to further precisely control the location of Au-coated areas at the substrate. As expected, the cross-aligned NW arrays were selectively formed on the Au-coated areas. By manipulating the geometries of Au-coated areas, different patterns of cross-aligned NW arrays, with shapes ranging from grid-like structures to complex labels ("FUNSOM"), were successfully obtained (Figure 3). Furthermore, the densities of the NW arrays were readily controlled by adjusting the growth conditions. Figure S6a and S6b present the SEM images of the NW arrays grown under 2×10^3 and 2 Pa, respectively. The NW arrays grown at a lower pressure are much denser due to the higher evaporation velocity of the CuPc source. The desired patterns can be achieved over large areas using this method, which is of great importance in practical device applications.

In current nanotechnology, device integration is usually hindered by the difficulties of NW manipulation and alignment. The present one-step method of large scale patterning cross-aligned organic NW arrays selectively on Au-coated areas makes the in-situ device integration possible. An image sensor circuitry with high integration level was successfully achieved using a pre-fabricated sensor circuit. The sensor circuit composed of 10×10 pixels (1.3×1.3 mm^2 in area),

was first pre-defined on a SiO$_2$ (300 nm)/p$^+$-Si substrate *via* multi-step photolithography and metallization (Figure S7 and Figure 4a–4b). Photoresist windows were then opened so that the NW arrays could selectively grow on the regions of Cr (5 nm)/Au (50 nm) electrodes (Figure 4c). Figure 4d shows the optical image of the sensor circuit with photoresist windows at each pixel. After growth, every pixel was covered by the dense CuPc NW arrays due to the template effect of the Au electrodes, while no NW arrays were observed on the photoresist surface, as shown in Figure 4e–4g. It should be noted that NW growth and device integration were accomplished simultaneously, which avoided the complicated NW manipulation/alignment process for integration. The relatively low processing temperature ($\sim 180^\circ$C) also ensured the NW growth and device integration safely. Although the alignment of the NW arrays was not as perfect as that on the thin Au film-coated Si substrate due to the uneven substrate surface and the thick Au layer on the electrode, the NW arrays were still relatively uniform from pixel to pixel. Each pixel contained hundreds of crossed NWs over the electrode pair. Although the CuPc NWs were not directly bridged over the electrode pairs on the plane, they crossed each other and formed the three-dimensional (3D) conduction channels between the electrode pairs. In conventional planar devices, NWs lie on the substrate plane
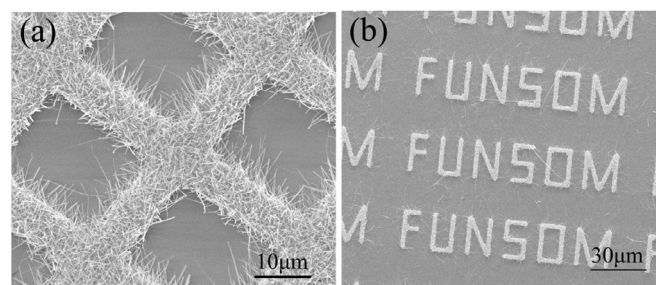
Figure 3 | Selective growth of CuPc NW array on various Au patterns on Si substrate, including (a) grid-like structure and (b) the label of "FUNSOM".
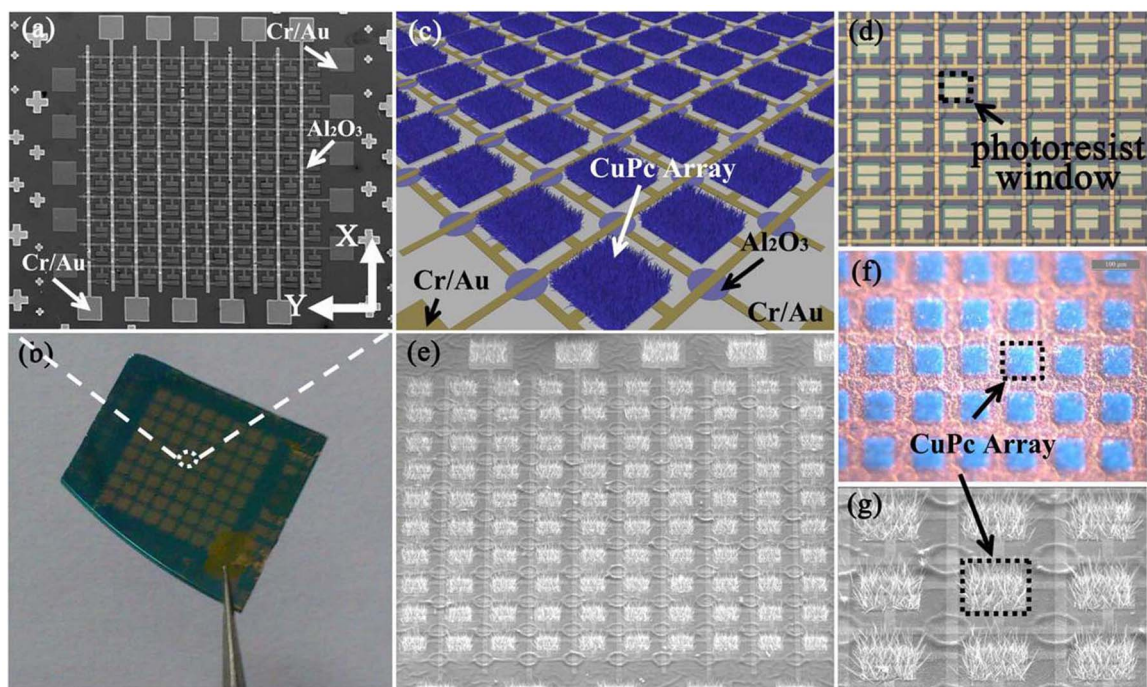
Figure 4 | (a) SEM image and (b) optical photograph of the as-fabricated sensor circuitry, which has 1.3×1.3 mm² surface area containing a 10×10 pixel array. (c) Schematic illustration of the image sensor circuit based on crossed CuPc NW arrays. (d) Optical photograph of the device cricuit before NW arrays growth. The dashed box in (d) indicates one of the photoresist windows opened on the pixel regions for achieving the localized growth of the NW arrays. (e) SEM image of the device. The CuPc NW arrays can selectively grow on the pixel regions. (f) Optical photograph of the device after NW arrays growth. CuPc NW arrays have blue color in the photograph. (g) Enlarged SEM image of the NW arrays on the pixels. The NWs cross each other and form 3D conduction channels between the electrode pairs.

and the light absorption length is equal to the NW length between the channels[30,31]. Due to the limited effective absorption length in these devices, the light absorption is less efficient, resulting in a limited photocurrent. In a remarkable contrast, the light absorption length in the crossed NW array-based photodetectors is extended throughout the entire length of the crossed NWs, which is usually longer than tens of micrometers. Another important advantage of the crossed NW arrays is the strong light-trapping effect, which, combined with the extended light absorption length, endow these NW arrays great potentials for applications as high-performance optical sensors. In addition, compared with a single NW, the NW array acting as a sub-unit can enhance the yield and reduce the variation by taking advantage of the averaging effect[6]. For the single organic NW based device, the contact issue, along with the variation of NW dimension, usually leads to the poor reproducibility of the device. Also, its device current is too low to meet the requirement for practical applications and complex amplifying circuit is needed. By contrast, the direct growth of cross-aligned NW array on electrode pairs can ensure a good electrical contact. Moreover, the high uniformity of the NW array is conducive to the improvement of the pixel yield. With much enhanced photocurrent, the signal from the NW array based device is easier to collect. From the SEM investigation (Figure S8), we note that crossed NWs connect each other through physical contact, rather than fusing together at contact point. This fact can be understood by the growth mechanism of the NWs; the growth of CuPc NWs was initiated and sustained at the NW/Au NP interface, therefore the growth rates at NW tops and sides were very low. As a result, even though the NWs contacted each other during NW growth process, they would not fuse together because the growth does not happen at the contact point. It is noted that the contact resistance may exist for the crossed NWs in such kind of device architecture. However, its impact on device performance is not so obvious, which can be judged from the linear *I-V* curves of the device (discussed below).

Prior to evaluate the operational performance of the image sensor, the *I-V* characteristics of an individual circuit element under dark, constant, and on-off modulated light illumination conditions were detected, as shown in Figure 5. The dark and light resistance for NW-array-based device were measured to be 6.4×10^{10} Ω and 9.7×10^{9} Ω respectively, giving rise to an I_{light}/I_{dark} ratio of ~7 (Figure 5a). The relatively low I_{light}/I_{dark} ratio can be attributed to (i) the large dark current caused by the large number of NWs across the conduction channel, and (ii) the longer carrier transport path and the existence of grain boundary in the crossed NW array structures and thus a stronger carrier recombination. To illustrate this, photo-response of both single-NW and multi-NW based planar devices were detected, as shown in Figure S9. It is noted that the single-NW device has a low dark current of $\sim5 \times 10^{-13}$ A at $+15$ V, giving rise to a high I_{light}/I_{dark} ratio of 60. In contrast, the dark current for the multi-NW based device is increased to $\sim1.2 \times 10^{-10}$ A at $+15$ V, while the photocurrent was not enhanced proportionally due to the defects and contact issues, thus resulting in a small I_{light}/I_{dark} ratio of about 4. This result manifests that the large dark current of the CuPc NW array based device was mainly determined by the large number of NWs across the device channel, and seemed to have no relation with its 3D device architecture. One possible solution to enhance the I_{light}/I_{dark} ratio is with introduction of Schottky or p-n junction structures in the devices[32,33]. As in the preliminary study shown in Figure S10 and S11, we fabricated the CuPc NW array based optical sensors on Ti-Au and Ti-Ti electrodes pairs using the same method, Ti electrode with lower work function (4.33 eV) can form Schottky junction with CuPc NW array. The dark current of the devices are greatly suppressed due to the existence of Schottky barrier at the interface, resulting in a remarkable enhancement in the switching ratio of 60 and 125 for Ti-Au and Ti-Ti electrode pairs, respectively.

The time-resolved photo-response measurements were conducted under pulsed light illumination, as depicted in Figure 5b, with an external bias voltage on the pixel fixed at $+15$ V. The current sharply

4
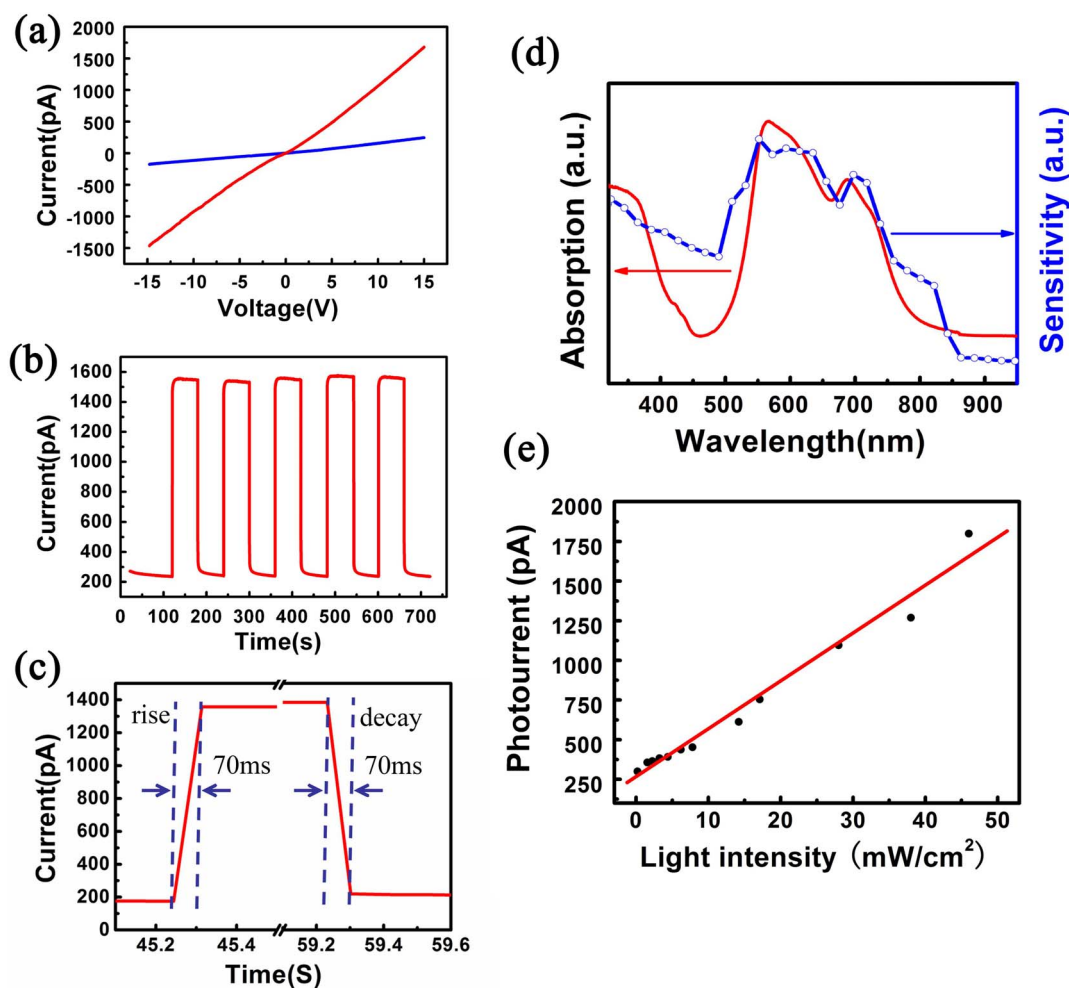
Figure 5 | (a) *I-V* characteristics of one of the pixels under dark and light illumination. A red laser diode was used as the light source. (b) Photoconductive response of the pixel under on-off modulated laser illumination. The voltage bias was fixed at +15 V. (c) Enlarged view of the rise and decay edges of the photoresponse spectrum. (d) Wavelength-dependent sensitivity of the device, along with the UV-vis absorption spectrum of the CuPc NW array for comparison. (e) Light intensity-dependent photocurrent.

increased when the light was turned on and remained constant until the light power was turned off, at which point the current rapidly reverted to the original dark current. Figure 5c shows the enlarged view of the rise and decay edges of the response curve. The measured response time of the CuPc NW array at one pixel was below 70 ms, which could not be accurately determined due to the instrumental limitations. However, the response time obtained is adequate for this study, and theoretically has enough scope to improve the switching speed of the device in the future, if desired. Notably, the device showed nearly identical photo-response for multiple response cycles, revealing the high stability, good reproducibility, and robustness of the NW array for optical sensor applications. Figure 5d displays the wavelength-dependent sensitivity of an individual sensor pixel. The response spectrum of the device is in good agreement with the absorption spectrum, implying that the electron-hole pairs excited by the incident light are responsible for the photocurrent generated in the device. The NW array showed a higher sensitivity in the range of 500–800 nm, as well as an increased response in the short wavelength direction (<500 nm). These results indicate that the CuPc NW array-based optical sensor can serve as a wide-band detector with the detection wavelength spanning from ultraviolet to near infrared. The light intensity-dependent photocurrent is depicted in Figure 5e, indicating the near linear relationship of photocurrent with light intensity.

To validate the function of sensor circuitry as an image sensor, we used the white light emitted from the optical microscope on the probe station as the light source to obtain an even light field on the device (light intensity was 15 mW·cm^{-2}). The measured dark current and photocurrent, which represent the background signal level and the light intensity level at each pixel, respectively, were incorporated into a two-dimensional (2D) plot to generate contrast maps, as shown in Figure 6a and 6b, respectively. Significantly, 100% of the pixels successfully operated and a majority of the pixels showed the closed sensitivity (Figure 6c and 6d), revealing the average dark and light currents of 343 and 1128 pA, respectively. The photocurrent had a standard deviation of ±164 pA. The slightly different responses may be induced by the fluctuation in the NW number and electrical contact quality. It should be emphasized that the 100% yield of the device has surpassed those of image sensors fabricated from parallel-aligned inorganic NW arrays in previous studies, which generally presented yields lower than 80%[27,28]. The relatively small pixel-to-pixel variation of the sensor fabricated in the present study arose from the high uniformity of the organic NW arrays. The direct growth of organic NW arrays on the sensor circuit also ensures a high contact quality between the NWs and the electrodes. The high yield of the operational pixels, along with the high integration level of the device, clearly demonstrates the great potential of the one-step organic NW array growth and device construction approach for large-scale optoelectronic device integration.

Owing to the unique read-bus structure of the sensor circuitry, the large electrode pads in the conventional sensors with discrete device
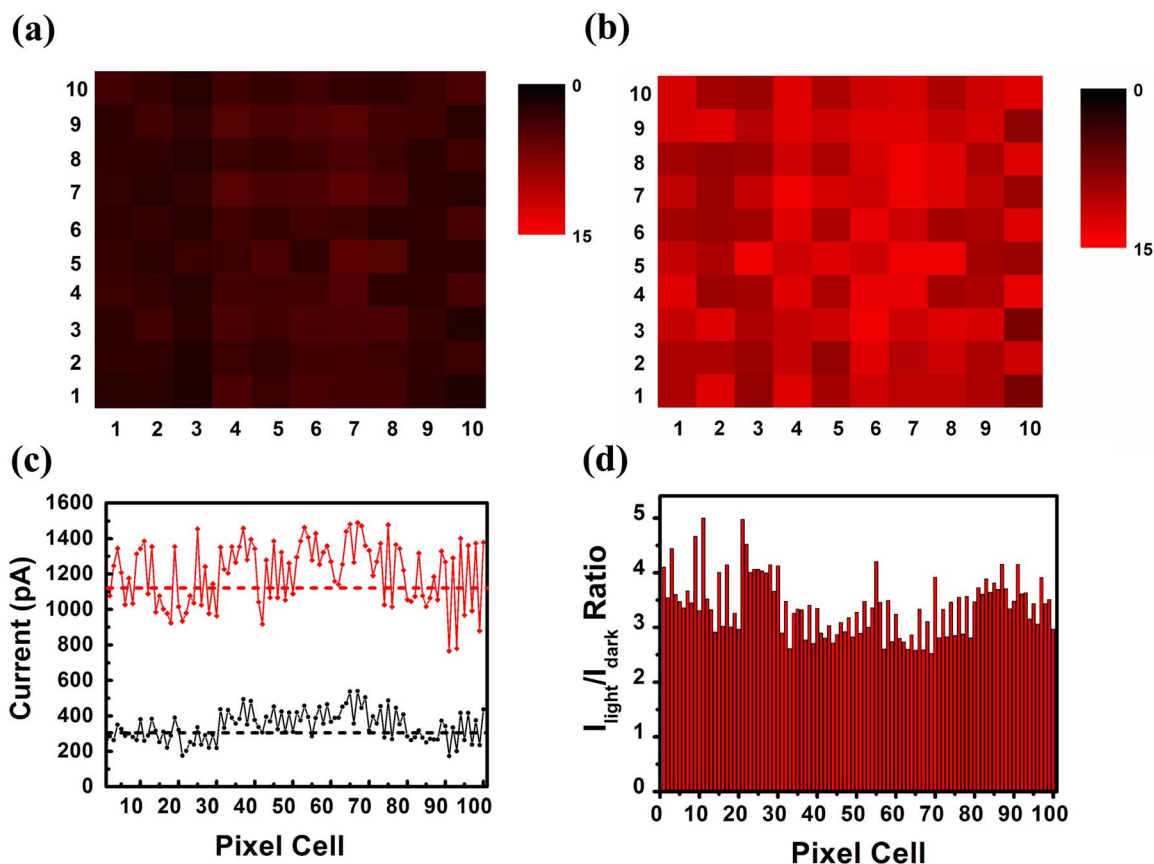
Figure 6 | Contrast maps showing the functional circuit elements (a) in the dark and (b) by exposing the device to an even light field. The white light emitted by the optical microscope on the probe station was used as the light source. (c) Dark current and the corresponding photocurrent for each pixel. The dash lines represent the average values for dark current (black) and photocurrent (red). (d) The diagram shows the I_{light}/I_{dark} ratio at each pixel.

structures were replaced by the read-bus in X and Y directions. Therefore, the integration level of the device was significantly improved, enabling the circuit matrix to function as a high-resolution image sensor. In this study, the surface area for each pixel was about 130×130 μm². By contrast, the pixel size was rather larger in previous reports due to the discrete device structure ($>800 \times 800$ μm²)[27,28]. A red laser beam with a point diameter of ~1 mm was projected onto one of the corner of the sensor circuitry to demonstrate the feasibility of the device as a high-resolution image sensor (Figure 7a). The output current was measured for each pixel and digitized into a 0–50 scale with "0" and "50" representing the minimum and maximum measured intensities, respectively. Therefore, a 2D image was constructed, as shown in Figure 7b. It is seen that the spatial intensity distribution in the contrast map exactly matches the shape of the laser beam. Only the devices in the corner position exhibited pronounced photoresponse, whereas the rest of the devices showed weak photocurrent output. This result clearly demonstrates the preliminary imaging function of the CuPc NW arrays.

Conclusion

In summary, we reported one-step patterned growth and device integration of cross-aligned single-crystalline organic NW arrays for high-performance optical imaging circuitry in a large-area. The cross-aligned NW arrays can selectively grow on Au film-coated areas induced by the high surface energy. NW array patterning and device integration can be obtained simultaneously by manipulating the Au electrode geometries on the substrate by photolithography. The integration level of the image sensor was remarkably improved using a unique read-bus architecture. A 10×10 pixel array with an area of 1.3×1.3 mm² was achieved, enabling the circuit

matrix to function as a high-resolution image sensor. Higher integration level is expected to be achieved by further reducing the pixel size in future study. Notably, the one-step device fabrication produced an image sensor with high reliability and high yield. One hundred percent of the image pixels worked properly with a very quick response speed of ~70 ms. The one-step organic NW array growth and device integration is expected to have important applications in new-generation nanoelectronic and nano-optoelectronic devices.

Methods

Synthesis and characterization of CuPc NW arrays. Synthesis of the CuPc NW arrays was conducted in a horizontal quartz tube furnace *via* a physical vapor deposition (PVD) method using Au NPs as the growth templates. The Si (100) substrates were first ultrasonically cleaned in acetone and alcohol for 10 min, respectively, and then a seed layer composed of 6 nm Au film was deposited on the clean Si substrates by high-vacuum electron beam (e-beam) evaporation (PVD 75, Kurt J. Lesker). A predetermined amount of α-phase CuPc powder (30 mg, J&K, purity > 90%) was mixed with the Al_2O_3 absorbent (1.5 g, 100–200 mesh) and then placed at the high temperature zone of the furnace, while the Au-coated Si substrates were placed at the downstream positions ~20 cm from the source material. After the tube was evacuated to a base pressure of 2 Pa, a carrier gas of high-purity Ar (99.99%) was fed at a constant flow ratio of 60 sccm. The pressure in the tube was adjusted to 220 Pa during the experiments. Thereafter, the source material was heated to 415°C at a rate of 20°C/min and then maintained at this temperature within a given time. The substrate temperature was ~180°C. The as-synthesized CuPc NW arrays were blue in color, which is consistent with the color of the source material. Besides CuPc NW arrays, $F_{16}CuPc$ and PTCDA NW arrays were also fabricated under the same growth conditions by using the Au-templated method. Furthermore, 8 nm Ag film, instead of Au film, was used to fabricate the CuPc NW arrays under the same conditions.

The morphologies of the products were characterized by SEM (FEI Quanta 200F). The phase and crystallography of the products were detected using a TEM (Philips CM300) operated at an acceleration voltage of 80 kV with SAED. The UV-vis
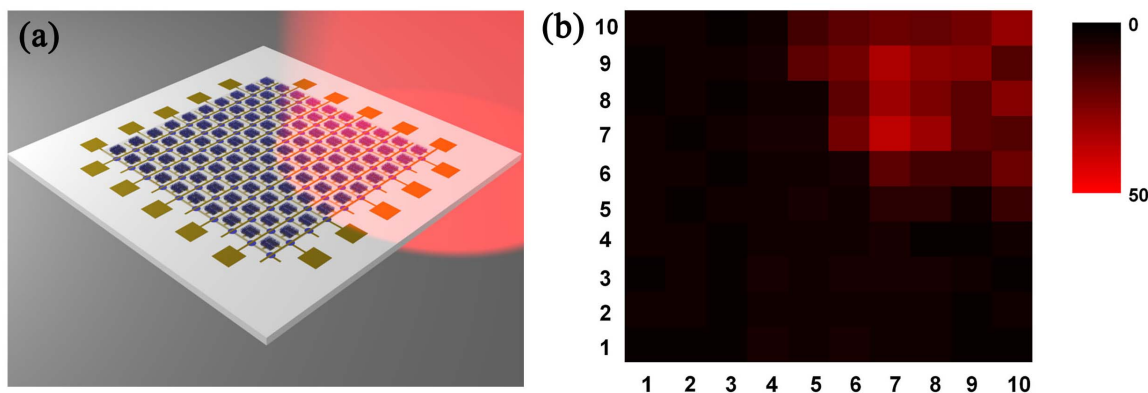
Figure 7 | (a) Schematic illustration of the measurement configuration for examining the capability of the sensor for spatial imaging. A red laser beam was projected onto the right-upper corner of the circuit array. The corresponding 2D intensity profile measured by mapping the pixel signals is shown in (b), imaging a quarter of circular light spot.

absorption spectrum was measured using a spectrometer (UV-VIS-NIR, PerkinElmer Lambda 750).

Construction of optical image sensor based on CuPc NW arrays. To construct the image sensor, the sensor circuit consisting of 10 × 10 pixels with an area size of 1.3 × 1.3 mm^2 was fabricated on the SiO$_2$ (300 nm)/p$^+$-Si substrate *via* microfabrication. At first, read bus in the X direction, together with the electrode pairs with gap of 5 µm for each pixel, was fabricated by photolithography using positive photoresist (AR-P 5320) and followed by a lift-off process. The thickness of the photoresist was about 1 µm. Cr (5 nm)/Au (50 nm) electrodes were used and deposited by e-beam evaporation. After that, the circle photoresist windows were defined by photolithography at the predetermined crossed positions of the X-bus with Y-bus. A thin Al$_2$O$_3$ layer (50 nm) was then deposited onto the photoresist windows using atomic layer deposition (ALD, Cambridge NanoTech) to serve as the insulative layer between the X-bus and Y-bus. In ALD deposition, trimethylaluminum (TMA) and pure water were used as precursors, and Al$_2$O$_3$ layer was deposited at 100°C for 600 cycles (~50 nm thick). Each cycle consisted of a 0.015-sec TMA precursor pulse, a 20-sec nitrogen purge, a 0.015-sec water vapor pulse, and then a 20-sec nitrogen purge. Eventually, the read-bus in Y direction was also fabricated by additional photolithography and lift-off process.

To realize the localized growth of CuPc NW arrays on sensor pixels, a new layer of photoresist (thickness 1 µm) was spin-coated on the whole sensor circuit and then square photoresist windows were opened on each pixel by photolithography. The sample was then subjected to argon plasma (power = 300 W, pressure = 0.3 Torr, time = 2 min) to eliminate the organic residue and solvent on the electrode pairs, thereby, ensuring an ohmic contact with the organic NW arrays grown later. The sensor circuit was placed into the tube furnace and the CuPc NW arrays were synthesized using the same method described previously. The growth duration was 1 h to guarantee an appropriate NW length.

All the electrical measurements were conducted using a semiconductor characterization system (Keithley 4200-SCS) on a probe station (M150, Cascade) in a clean and shielded box at room temperature. To determine the photoconductive characteristics of the CuPc NW arrays, a red laser diode with a center wavelength of 650 nm, beam diameter of ~1 mm, and intensity of ~50 mW·cm^{-2} was used as the light source. An illumination system composed of a Xenon lamp (500 W) and a monochromator was employed to provide monochromatic light for the measurement of the spectral response.

1. Nam, S. W., Jiang, X., Xiong, Q., Ham, D. & Lieber, C. M. Vertically integrated, three-dimensional nanowire complementary metal-oxide-semiconductor circuits. *Proc. Natl. Acad. Sci.* **106**, 21035–8 (2009).
2. Beckman, R., Johnston-Halperin, E., Luo, Y., Green, J. E. & Heath, J. R. Bridging Dimensions: Demultiplexing Ultra-High Density NanowireCircuits. *Science* **310**, 465–8 (2005).
3. Huang, Y., Duan, X., Wei, Q. & Lieber, C. M. Directed Assembly of One-Dimensional Nanostructures into Functional Networks. *Science* **291**, 630–3 (2001).
4. Cao, Q. *et al.* Medium-scale carbon nanotube thin-film integrated circuits on flexible plastic substrates. *Nature* **454**, 495–500 (2008).
5. McAlpine, M. C., Ahmad, H., Wang, D. & Heath, J. R. Highly ordered nanowire arrays on plastic substrates for ultrasensitive flexible chemical sensors. *Nat. Mater.* **6**, 379–84 (2007).
6. Takei, K. *et al.* Nanowire active-matrix circuitry for low-voltage macroscale artificial skin. *Nat. Mater.* **9**, 821–6 (2010).
7. Wong, W. S., Raychaudhuri, S., Lujan, R., Sambandan, S. & Street, R. A. Hybrid Si Nanowire/Amorphous Silicon FETs for Large-Area Image Sensor Arrays. *Nano Lett.* **11**, 2214–8 (2011).
8. Cui, Y., Lauhon, L. J., Gudiksen, M. S., Wang, J. & Lieber, C. M. Diameter-controlled synthesis of single-crystal silicon nanowires. *Appl. Phys. Lett.* **78**, 2214 (2001).
9. Jin, C., McLachlan, M. A., McComb, D. W., Richard, M. & Johnson, N. P. Template-assisted growth of nominally cubic (100)-oriented three-dimensional crack-free photonic crystals. *Nano Lett.* **5**, 2646–50 (2005).
10. Grimsdale, A. C. & Müllen, K. The Chemistry of Organic Nanomaterials. *Angew. Chem. Int. Ed.* **44**, 5592–629 (2005).
11. Zhang, X. J., Zhang, X. H., Zou, K., Lee, C. S. & Lee, S. T. Controlled Synthesis of Single Crystalline Nanoribbons, Nanotubes and Nanowires from Intramolecular Charge-Transfer Organic Molecules. *J. Am. Chem. Soc.* **129**, 3527–32 (2007).
12. de la Torre, G., Vazquez, P., Agullo-Lopez, F. & Torres, T. Role of Structural Factors in the Nonlinear Optical Properties of Phthalocyanines and Related Compounds. *Chem. Rev.* **104**, 3723–50 (2004).
13. Hirade, M., Nakanotani, H., Yahiro, M. & Adachi, C. Formation of Organic Crystalline Nanopillar Arrays and Their Application to Organic Photovoltaic Cells. *ACS Appl. Mater. Interfaces* **3**, 80–3 (2010).
14. Zhao, Y. S., Peng, A., Fu, H., Ma, Y. & Yao, J. Nanowire Waveguides and Ultraviolet Lasers Based on Small Organic Molecules. *Adv. Mater.* **20**, 1661–5 (2008).
15. Briseno, A. L. *et al.* Fabrication of Field-Effect Transistors from Hexathiapentacene Single-Crystal Nanowires. *Nano Lett.* **7**, 668–75 (2007).
16. Xiao, K. *et al.* Metastable Copper-Phthalocyanine Single-Crystal Nanowires and Their Use in Fabricating High-Performance Field-Effect Transistors. *Adv. Func. Mater.* **19**, 3776–80 (2009).
17. Xu, H. B., Chen, H. Z., Xu, W. J. & Wang, M. Fabrication of organic copper phthalocyanine nanowire arrays via a simple AAO template-based electrophoretic deposition. *Chem. Phys. Lett.* **412**, 294–8 (2005).
18. Zhang, Y. P. *et al.* Aligned ultralong nanowire arrays and their application in flexible photodetector devices. *J. Mater. Chem.* **22**, 14357–62 (2012).
19. Briseno, A. L. *et al.* Patterning organic single-crystal transistor arrays. *Nature* **444**, 913–17 (2006).
20. Zhao, Y., Zhan, P., Kim, J., Sun, C. & Huang, J. Patterned growth of vertically aligned organic nanowire waveguide arrays. *ACS Nano* **4**, 1630–6 (2010).
21. Zhang, C. Y. *et al.* Facile One-Step Growth and Patterning of Aligned Squaraine Nanowires via Evaporation-Induced Self-Assembly. *Adv. Mater.* **20**, 1716–20 (2008).
22. Zhang, C. Y. *et al.* Facile One-Step Fabrication of Ordered Organic Nanowire Films. *Adv. Mater.* **21**, 4172–5 (2009).
23. Wang, Z. L. *et al.* One-Step Self-Assembly, Alignment, and Patterning of Organic Semiconductor Nanowires by Controlled Evaporation of Confined Microfluids. *Angew. Chem. Int. Ed.* **50**, 2811–5 (2011).
24. Liu, Y. *et al.* Controlling the Growth of Single Crystalline Nanoribbons of Copper Tetracyanoquinodimethane for the Fabrication of Devices and Device Arrays. *J. Am. Chem. Soc.* **128**, 12917–22 (2006).
25. Xiao, K. *et al.* Growth, Patterning, and One-Dimensional Electron -Transport Properties of Self-Assembled Ag-TCNQF4 Organic Nanowires. *Chem. Mater.* **21**, 4275–81 (2009).
26. Tang, Q., Tong, Y., Hu, W., Wan, Q. & Bjørnholm, T. Assembly of Nanoscale Organic Single-Crystal Cross-Wire Circuits. *Adv. Mater.* **21**, 4234 (2009).
27. Ozgur, E., Aktas, O., Kanik, M., Yaman, M. & Bayindir, M. Macroscopic assembly of indefinitely long and parallel nanowires into large area photodetection circuitry. *Nano Lett.* **12**, 2483–7 (2012).
28. Fan, Z., Ho, J. C., Jacobson, Z. A., Razavi, H. & Javey, A. Large-scale, Heterogeneous Integration of Nanowire Arrays for Image Sensor Circuitry. *Proc. Natl. Acad. Sci.* **105**, 11066–70 (2008).
29. Zhao, Y. S., Wu, J. S. & Huang, J. X. Vertical Organic Nanowire Arrays: Controlled Synthesis and Chemical Sensors. *J. Am. Chem. Soc.* **131**, 3158–3159 (2009).

7

30. Zhou, Y., Wang, L., Wang, J., Pei, J. & Cao, Y. Highly Sensitive, Air-Stable Photodetectors Based on Single Organic Sub-micrometer Ribbons Self-Assembled through Solution Processing. *Adv. Mater.* **20**, 3745–9 (2008).
31. Zhang, X. J. *et al.* Photoconductivity of a Single Small-Molecule Organic Nanowire. *Adv. Mater.* **20**, 2427–32 (2008).
32. Peng, Q. *et al.* Nano-Schottky barrier diodes based on Sb-doped ZnS nanoribbons with controlled p-type conductivity. *Appl. Phys. Lett.* **98**, 123117 (2011).
33. Wu, D. *et al.* Device structure-dependent field-effect and photoresponse performances of p-type ZnTe:Sb nanoribbons. *J. Mater. Chem.* **22**, 6206–12 (2012).

Acknowledgments

Author contributions

Y.M.W., J.S.J., X.J.Z. wrote the manuscript. J.S.J., X.H.Z. and X.J.Z. were responsible for the overall experimental design. Y.M.W. and H.H.P. conducted the experiments, W.D. and X.W.Z. measured the devices. All authors reviewed the manuscript.

Additional information

Supplementary information accompanies this paper at http://www.nature.com/scientificreports

Competing financial interests: The authors declare no competing financial interests.

How to cite this article: Wu, Y.M. *et al.* In-situ device integration of large-area patterned organic nanowire arrays for high-performance optical sensors. *Sci. Rep.* **3**, 3248; DOI:10.1038/srep03248 (2013).